RESEARCH ARTICLE

ADVANCED
ELECTRONIC
MATERIALS
Open Access

www.advelectronicmat.de

Check for updates

Impact of Thermal Annealing on the Dissolution of Semiconducting Polymer Thin Films

Shaoling Bai, Katherina Haase, Jonathan Perez Andrade, Mike Hambsch, Felix Talnack, Vojtech Millek, Anupam Prasoon, Jinxin Liu, Kerstin Arnhold, Susanne Boye, Xinliang Feng, and Stefan C. B. Mannsfeld*

Here, the effect of thermal annealing (TA) on the stability of solution-sheared thin films of the semiconducting polymer poly[2,5-bis(2-octyldodecyl)-pyrrolo[3,4-c]pyrrole-1,4(2H,5H)-dione-3,6-diyl)-alt-(2,2′;5′,2′′;5′′,2′′′-quaterthiophen-5,5′′′-diyl)] (PDPP4T) against the original coating solvent is studied, and it is shown that TA significantly improves the solvent resistance of semiconducting polymer films. Specifically, after the thin films are annealed at or above a critical temperature, the thin film thickness is largely retained when exposed to the original solvent, while for lower annealing temperatures material loss occurs, i.e., the thin film thickness is reduced due to rapid dissolution. The results of various techniques including grazing-incidence wide-angle x-ray scattering (GIWAXS), atomic force microscopy (AFM), and ultraviolet-visible-near infrared (UV–vis-NIR) absorption spectroscopy suggest physical changes as the cause for the increased solvent resistance. Such annealed films also show stable electrical characteristics in bottom-gate, top-contact (BGTC) organic field-effect transistors (OFETs) even after solvent exposure. In initial tests, a multitude of technologically relevant polymers show such behavior, underlining the potential impact of such temperature treatments for the fabrication of multi-layer polymer devices.

1. Introduction

Multi-layer organic devices are appealing candidates for next-generation flexible and wearable electronics since they are promising in innovative and versatile devices such as multiple color emitting diodes, flexible solar cells, and novel memory devices.[1–9] Compared with thermal evaporation, which is a common method to fabricate organic multilayer small molecule devices, solution processing exhibits many advantages including low-cost, compatibility with both small molecules and polymers, and large-area fabrication. To produce electronic devices with multiple layers of soluble organic functional materials such as electrodes, semiconductors, and dielectrics, solvent orthogonality is required to protect the underlying layer, which represents a significant processing limitation.[10,11] In addition, these methods do not match with photolithography processing, which is one of the fundamental technologies in the present silicon semiconductor industry. Therefore, several studies investigated cross-linking methodologies to fabricate solvent-stable semiconducting polymer films. However, these often involve UV light exposure to trigger the cross-linking reaction of cross-linkers with multi-functional groups, which is often harmful to the performance of the fabricated semiconducting polymer-based devices.[9,12] Hence, physical cross-linking, side chain cleavage, and semiconducting polymers with active cross-linking groups are emerging as promising strategies for preparing solvent-stable semiconducting films.[7,8,13]

For almost any of these strategies, some sort of post-thermal annealing is indispensable, not only in conjunction with

S. Bai, K. Haase, J. Perez Andrade, F. Talnack, V. Millek, S. C. B. Mannsfeld
Faculty of Electrical and Computer Engineering
TUD Dresden University of Technology
01062 Dresden, Germany
E-mail: katherina.haase@tu-dresden.de;
stefan.mannsfeld@tu-dresden.de

S. Bai, K. Haase, J. Perez Andrade, M. Hambsch, F. Talnack, V. Millek,
A. Prasoon, J. Liu, X. Feng, S. C. B. Mannsfeld
Center for Advancing Electronics Dresden (cfaed)
TUD Dresden University of Technology
01062 Dresden, Germany

A. Prasoon, J. Liu, X. Feng
Faculty of Chemistry and Food Chemistry
TUD Dresden University of Technology
01062 Dresden, Germany

K. Arnhold, S. Boye
Center Macromolecular Structure Analysis
Leibniz-Institut für Polymerforschung Dresden e.V
Hohe Straße 6, 01069 Dresden, Germany

**ADVANCED
SCIENCE NEWS**

www.advancedsciencenews.com

**ADVANCED
ELECTRONIC
MATERIALS**

www.advelectronicmat.de

cross-linking, but also as a process step for removing residual solvent, increasing the crystallinity of organic thin films, and notably improving device electrical properties.[14–20] It has been widely studied how thermal annealing can change the microstructure and crystallinity of organic semiconducting thin films.[21–26] However, there are no reports on thermal annealing influencing the solvent resistance of semiconducting polymer films.

Here, we investigated the film stability of the commercial polymer PDPP4T after annealing at different temperatures by observing the morphological and thickness changes after the exposure to the original solvent that was used for thin film preparation. While the effect of thermal annealing on PDPP4T has been previously studied by Li and co-workers,[27] emphasizing its effect on OFET mobility, the impact of thermal annealing on thin film stability during subsequent solvent exposure has so far not been reported. Specifically, we find that at temperatures commonly used for thermal annealing, thin films show strongly enhanced retention ($R = \frac{d_{after\ solvent}}{d_{before\ solvent}} \cdot 100\%$) when exposed to the same solvent that was used to deposit them. Furthermore, for relatively short solvent exposure times such as during spin-coating, temperatures compatible with common plastic substrates are sufficient to retain most of the film and hence, the process might be optimized for the use with flexible substrates.

To elucidate the mechanism of improved film resistance, we perform ex and in situ GIWAXS experiments. The microstructural changes in the films are further investigated with UV–vis absorption, Fourier-transform infrared (FT-IR), and Raman spectroscopy, as well as AFM measurements. Thermal analysis via thermogravimetric analysis (TGA) and differential scanning calorimetry (DSC) are further conducted. Based on our analysis, we conclude that the enhanced solvent resistance is at least partially related to changes in the microstructure of the films. While the mechanism is currently further investigated, we believe that this rather simple thermal annealing protocol represents a promising step for the fabrication of complex multilayer devices, which we support through tested OFETs. Specifically, BGTC transistors with thermally stabilized thin films retain good performance when mimicking an additional solution-processing step. Furthermore, top-gate OFETs with the dielectric layer deposited from the same solvent as used for semiconductor deposition show good characteristics. Finally, initial studies on other polymers suggest that similar changes can be obtained for other commonly used semiconducting polymers.

2. Results and Discussion

We first study the stability of semiconducting polymer thin films against their original solvent after annealing them at different temperatures. **Figure 1** shows the chemical structure of the investigated polymer (Figure 1a) and the retention R dependent on the annealing temperature (Figure 1b). In this experiment,

X. Feng
Department of Synthetic Materials and Functional Devices
Max Planck Institute of Microstructure Physics
Weinberg 2, 06120 Halle, Germany

all films were annealed for 20 min in a nitrogen-filled glovebox. The use of a nitrogen atmosphere to prevent degradation is in line with previous investigations on the thermal annealing of this polymer.[27] While we found that annealing in vacuum yielded similar results, for practical reasons, any annealing of films presented here was performed in nitrogen. As shown, the stability was tested by determining thin film retention upon exposure to the original solvent chloroform, and observation of morphology changes via optical microscopy. Specifically, the samples were exposed to their original solvent in various ways to emulate different subsequent solution processes including spin-coating, shear-coating, and dip-coating as it is commonly done to test the stability of cross-linked polymer semiconductors.[28,29] In Figure S1 (Supporting Information) we show photographic images of differently annealed films before and after exposure to their original solvent and microscopy images are shown in Figure 1d and Figure S2 (Supporting Information). It is clearly visible that the solvent stability of films improved enormously after annealing at high temperatures.

To visualize our data as well as to extract a meaningful metric that allows for comparison of different procedures, we fitted logistic functions to the data: $R(T) = \frac{R_{max}}{1 + e^{-k\ (T - T_{50})}}$. Here, $R(T)$ is the film thickness retention when the film had been annealed at the temperature T, T_{50} denotes the sigmoid midpoint where half of the maximum achievable retention R_{max} is observed (ideally 50% of original film thickness), and k is the growth rate or steepness of the curve, indicating how fast retention changes from zero to maximum when increasing the annealing temperature. In the context of our research, k thus describes how rapidly the physiological transformations in the films occur that produce the observed changes in dissolubility.

It can be seen that for all exposure tests, the film retention changes from 0% (no retention) to values equal to or greater than 92%. We further note that retention critically depends on the subsequent solvent treatment, particularly the solvent exposure time, which is different for the various exposure tests (dip-coating > shear-coating > spin-coating). Specifically, T_{50} temperatures of 143, 197, and 213 °C were obtained for samples exposed to the original solvent via spin-coating, shear-coating, and dip-coating, respectively. To determine an onset annealing temperature at which the solvent stability of the film begins to change, we extrapolate a fitted linear curve around T_{50} to zero and maximum retention. For the only short solvent exposure times, as emulated when chloroform was spin-coated onto the annealed samples, the onset temperature corresponded to 137 °C. When the annealing temperature was lower, most of the films were washed off and the residual films were very thin (below 5 nm). Hence, without sufficient solvent orthogonality no sequential solution-coating step could be feasible if the films would be only annealed at or below this temperature. Above this temperature, a subsequent process could be chosen according to the required retained film thickness, which itself could be estimated from $R(T)$.

Besides thickness retention, we further investigated the surface morphology change upon subsequent solvent exposure. It is seen that even when the films are (partially) retained, surface morphology is clearly affected. This is easily observed through the optical microscopy images, as shown in Figure S2 (Supporting Information). On the contrary, the surface morphology did not exhibit noticeable microscopic changes after the subsequent

**ADVANCED
SCIENCE NEWS**

www.advancedsciencenews.com

**ADVANCED
ELECTRONIC
MATERIALS**

www.advelectronicmat.de

solvent treatments for annealing temperatures ≥225 °C (t_{anneal} = 20 min), which is common for all – spin-coated, shear-coated, and immersed films. Above this temperature, films remain stable over rather long solvent exposure times and are not fully dissolved even after 24 h immersion in the original solvent. (Figure S3, Supporting Information).

We note that the solvent stability of films also depends on the annealing time (Figure S4, Supporting Information). As can, for instance, be seen from Figure S2 (Supporting Information), at an annealing temperature of 225 °C and annealing times shorter than 20 min, a clear effect on the surface morphology is seen after immersion in the original solvent and very short annealing times lead to lower film retention (Figure S4c, Supporting Information). On the contrary, at 250 °C, the same is not observed when the annealing time is reduced. Notably, an annealing time of only 1 min can be sufficient to introduce the required changes to distinctly slow down the dissolution of films.

Based on the observed changes in film properties we define three regimes, which are roughly indicated in Figure 1 I) a low-temperature regime, where the films have no solvent stability and immediately dissolve when exposed to their original solvent, II) a transition regime at intermediate annealing temperatures, where we observe a drastic change in the solvent resistance, but with noticeably affected surface morphology and stability towards short exposure times only, and III) a high-temperature regime, where the films appear solvent stable for extended times with minor effects on the surface morphology.

While the solvent-exposure and thermal annealing-time dependence of retention makes it difficult to pinpoint a specific temperature at which solvent resistance change occurs, we set out to explore the changes in the film structure starting to occur at intermediate thermal annealing temperatures and leading up to prolonged solvent resistance at high temperatures. Particular attention is given to the region at around 140 °C, where we approximate the onset of noticeable changes from the shortest solvent exposure times.

2.1. Thermal Transitions and Stability of PDPP4T

To identify the thermal transitions specific to the material we conducted DSC measurements. The results are shown in Figure S5 (Supporting Information). For PDPP4T, we determine the melting temperature T_m from the first and second heating curves ≈335 and 328 °C, respectively, which is close to reported literature values.[30] We also observe a shoulder of the peak in the first heating curve at a slightly lower temperature (315 °C). The existence of such shoulders or even double peaks has been attributed to the existence of different crystal phases/ presence of two distinct crystal populations[31] as well as the occurrence of melting–recrystallization–remelting mechanisms of small-sized crystals.[32,33] While we do not know the origin of the shoulder, we note that the onset of the melting transition lies in the evaluated temperature range for thermal annealing (>250 °C) and is expected to cause differences in morphology, which was studied through GIWAXS, UV–vis absorption spectroscopy and others. We further point out that the melting endotherm in the second heating curve is reduced from 34.7 to 28.2 J g^{-1} and peaks at slightly reduced temperature, which indicates lower crystallinity

and could hint toward the degradation of the material after heating to 350 °C.

We further note that we were unable to obtain T_g from this measurement, which is difficult for semicrystalline (conjugated) polymers in general.[34] Yet, according to the findings by Hajduk and co-workers who combined variable-temperature spectroscopic ellipsometry and DSC, the glass transition temperature of this PDPP4T batch (M333, Ossila) should be ≈70 °C (T_g = 69 °C, obtained from powder).[30] Furthermore, when measurements on the bulk material and films were compared, additional thermal transitions were seen for the latter. Specifically, several glass transition temperatures were determined (T_{g1}-T_{g3} = 32, 69, and 129 °C), which are known to arise from conformational changes of side chains and different amorphous phases, i.e., mobile and rigid amorphous fractions (MAF and RAF), as reported in other studies.[35,36] We conclude that rigid and mobile amorphous fractions might also exist in our thin films. However, the application of alternative measurement procedures is necessary to detect these different thermal transitions and obtain knowledge about their relative quantity.[37–40]

To understand whether the observed changes in solvent resistance were caused by side chain cleavage or degradation in general, we further conducted TGA. Figure S6 (Supporting Information) shows the result of the TGA measurement, wherein we find two peak temperatures, one ≈323 °C and one at 440 °C. Even though the onset of the first transition lies in the temperature range used for annealing, the weight loss of this transition is less than 1% (0.65%) at the final temperature (T_{final} = 360 °C) of this decomposition step. Hence, we find it unlikely that the solubility decrease of high-temperature annealed films is a result of thermal removal of solubilizing side chains. It appears more likely that the side chains are removed during the first of two following mass loss transitions apparent as a shoulder at 415 °C and a peak at 440 °C. This kind of double transition has for instance been reported for the polymer (poly[[4,8-bis[(2-ethylhexyl)oxy]benzo[1,2-b:4,5-b′]dithiophene-2,6-diyl][3-fluoro-2-[(2-ethylhexyl)carbonyl]thieno[3,4-b]thiophenediyl]]) (PTB7)[41] with the shoulder being attributed to the thermal cleavage of side chains.

To further support this, we also performed FT-IR spectroscopy (Figure S7, Supporting Information). No changes are observed concerning the aliphatic C-H stretching peaks upon annealing that could be interpreted as side-chain cleavage even at high temperatures. Hence, FT-IR data additionally confirms the absence of side-chain cleavage. The FT-IR data further shows a relative change of the vibrations at 710 and 733 cm^{-1} with the former attributed to the (CH$_2$)-n bending mode[42] and the latter being assigned to the imide ring deformation (Figure S7b, Supporting Information). Interestingly, as will be discussed later on, this change follows the same trend as seen in GIWAXS and UV–vis absorption spectra with a maximum change at 250 °C and its slight reversal at 300 °C. In addition to the absence of other indications, the latter observation makes us believe that this change is not due to a permanent chemical change, but rather related to the morphological changes that are also observed through other measurements. The same assumption is made for the slight red shift that is observed for these peaks above room temperature.

Finally, we would like to mention that we also collected complementary Raman spectra of differently annealed PDPP4T films
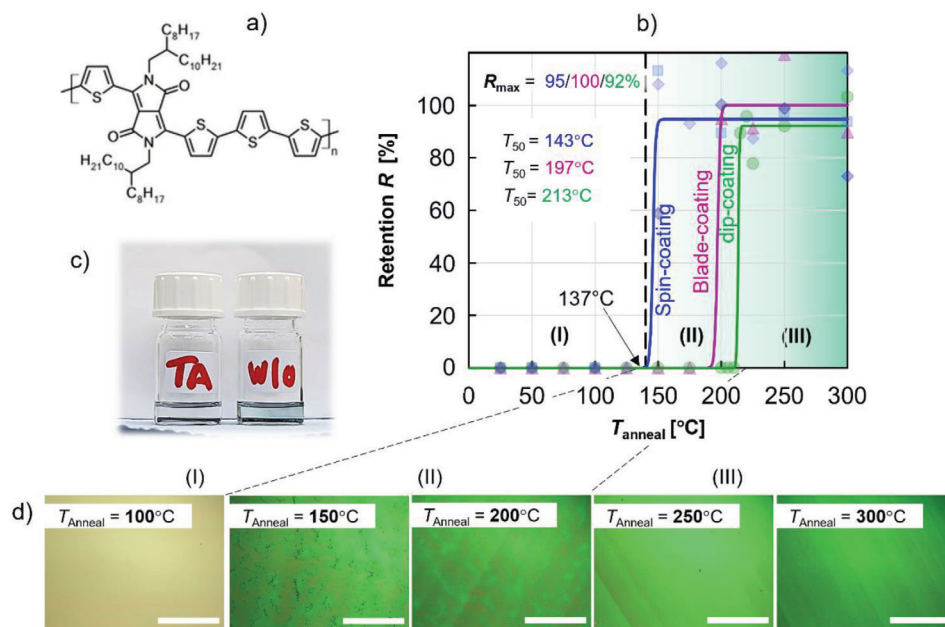
**ADVANCED
SCIENCE NEWS**

www.advancedsciencenews.com

**ADVANCED
ELECTRONIC
MATERIALS**

www.advelectronicmat.de

Figure 1. a) Chemical structure of PDPP4T, b) fitted retention R of PDPP4T thin films after different chloroform exposure tests (spin-coating, shear-coating, dip-coating) dependent on the thermal annealing temperature (annealing time = 20 min): $R(T) = \frac{R_{max}}{1 + e^{-k(T - T_{50})}}$; data points represent retention calculated from the average of five measurements before and after subsequent solvent exposure; c) photograph of immersed sample without (w/o) and with thermal annealing (TA), d) microscopy images of films annealed at different temperatures taken after post-anneal solvent exposure via spin-coating chloroform (scale bars: 500 µm).

(Figure S8, Supporting Information), which are consistent with other data with no indication of polymer degradation upon temperature exposure until 300 °C.

2.2. Morphology of Pristine and Annealed Films Before and After Original Solvent Exposure

To further explore the reason for the higher solvent tolerance after annealing at temperatures above 140 °C, we thoroughly studied the physical thin-film properties through ex and in situ GIWAXS measurements, AFM, and UV–vis absorption spectroscopy.

2.2.1. GIWAXS Study

In **Figure 2** we show the results of a series of differently annealed PDPP4T films. All data was taken at room temperature, i.e., ex situ. From the 2D diffraction images in Figure 2a and Figure S9 (Supporting Information), we observe that the films are textured with the ordered lamellar peaks in the out–of–plane direction and the π–π stacking peak in the in-plane direction, while the texture is less pure for non-annealed and low-temperature-annealed films. In Figure 2b, we plot the full width at half maximum (FWHM) obtained from in-plane and out-plane cuts of two of the characteristic peaks, namely (010) and (200) over the annealing temperature. We find that the FWHM values of the peaks decrease with the increase of annealing temperature, indicating an increased size of crystallites or crystalline regions in the films after the post-annealing treatment. Annealed films further show

lesser peak broadening of ascending diffraction order suggesting decreased paracrystalline disorder in those films.[43] Peaks of all annealed films have higher intensity with an increasing trend until 250°, indicating an increase in the volume of the crystalline fraction in the sample. When the films were annealed above this temperature, the intensity decreased, which is attributed to partial melting. The lamellar packing distance of annealed films is also slightly smaller as compared to the reference films. The minimum distance is observed for films annealed at 250 °C. The opposite is the case for the π–π stacking distance. Here, we observe a more pronounced increase in distance in high-temperature annealed films with the maximum located at 250 °C. We further observe the disappearance of the arcing of the (100) peak for films annealed in the temperature range from 100 to 250 °C that stems from misalignment of grains from the surface normal. The arcing (100) reappears for films annealed at 300 °C, indicating the initial improvement of grain alignment and its deterioration as the annealing temperature gets closer to T_m.

To further explore the molecular packing changes upon annealing, we studied the films via in situ GIWAXS measurements as shown in **Figure 3**. Figure 3a,c plots the FWHM of the (100) and (010) peaks, respectively, while Figure 3b,d maps the (100) and (010) peak positions during the annealing cycle. Corresponding 2D diffraction images are available in Figure S10 (Supporting Information).

It can be seen that despite the practical differences between in- and ex situ annealing, specifically the limited heating and cooling rate of the equipment, the observed changes at the start and end of the in situ annealing cycle are consistent with the result obtained from ex situ measurements. During heating, both the
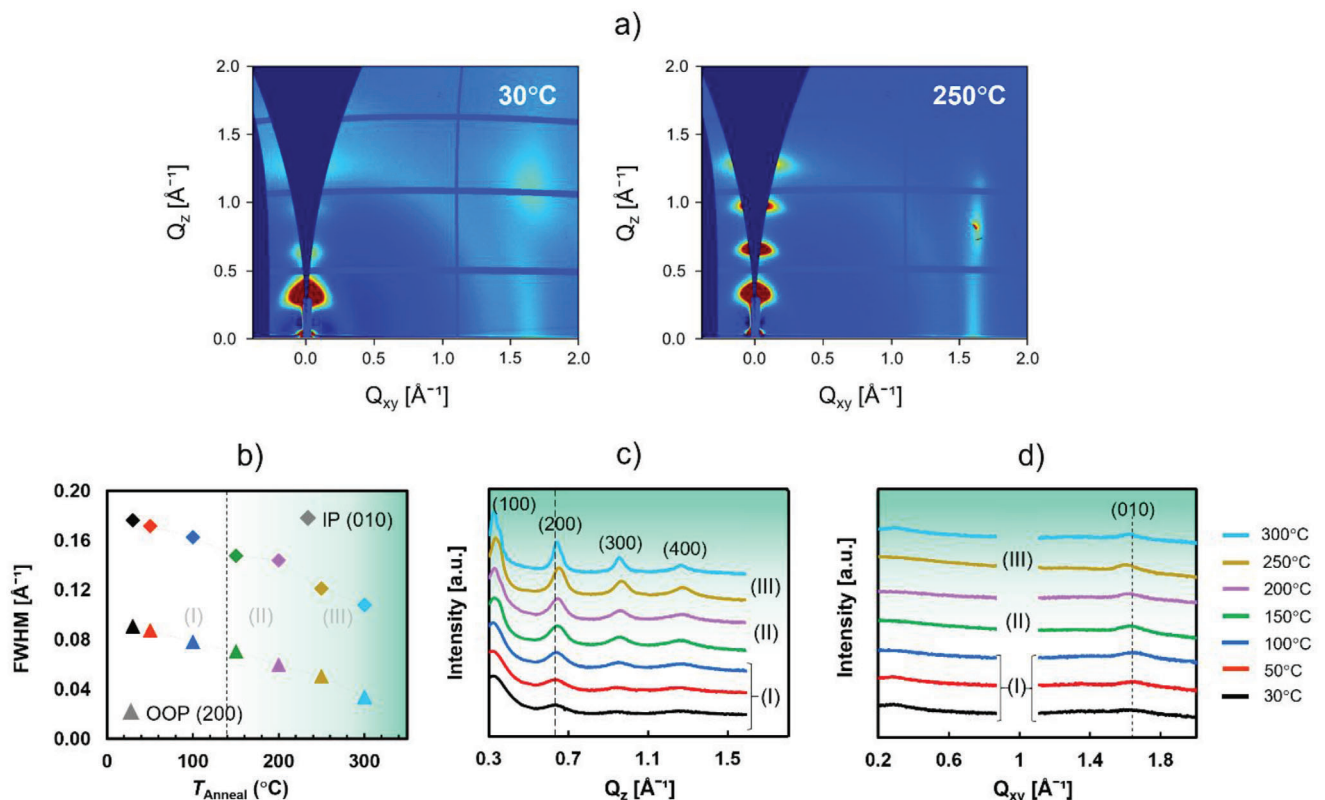
2300801 (4 of 14)

**ADVANCED
SCIENCE NEWS**

www.advancedsciencenews.com

**ADVANCED
ELECTRONIC
MATERIALS**

www.advelectronicmat.de

Figure 2. a) 2D scattering images of PDPP4T films comparing the microstructure after 20 min annealing at 30 and 250 °C (background-substracted); b) fitted FWHM values for the (010) in-plane peak (attributed to the π-π packing distance) and the second order out-of-plane peak (200). The values were obtained from Gaussian fits to the diffraction peaks with local background-subtraction; c) out-of-plane line cuts; d) in-plane line cuts obtained from 2D diffraction images (without background subtraction).

π−π stacking distance and the lamellar stacking distance increase, which is the result of thermal expansion and consistent with previous observations.[35] When the sample is slowly cooled down, both start to decrease again as the crystalline regions contract. While the π-π stacking distance does not return to its initial value, but instead remains higher after annealing, the lamellar stacking distance appears slightly reduced (although nearly the same as at the start of heating). Comparing the FWHM of the in-plane and out-of-plane peaks at the start and end of the temperature cycle, we can see the clear reduction after the annealing cycle. For the lamellar peak, the FWHM reduces strongly when heating up the sample and remains more or less constant during cooling down. In the case of the π−π packing peak, we observe the distinct reduction of the FWHM at the start of the cooling. Below 150 °C, it remains more or less constant.

Considering all – the in situ data (π−π peak FWHM), the absence of a distinctive exotherm in the heating curves of standard DSC measurements that could clearly indicate cold crystallization[32] and the onset of the melting transition (Figure S5, Supporting Information) – we infer that the increased crystallite size in films annealed at intermediate and high temperatures up to 250 °C most probably arises from crystallization of amorphous fractions during the initial cooling phase (250 °C → 150 °C) resulting in a film structure with overall larger grains. This is consistent with our in situ GIWAXS ex-

periments that do not indicate melting of the crystalline phase at 250 °C whereas such an indication does exist for the films that were annealed at 300 °C only (but measured ex situ after possible melt-crystallization) through their pronounced differences with respect to lower-temperature-annealed films., i.e., the appearance of arcing (100 peak) in the GIWAXS data, as well as the blue shift of the UV–vis absorption spectrum (see further below). This data suggests that films annealed at 300 °C partially melt and re-crystallize, which means that the "original" crystalline phase also contributes to the enhanced crystallite size after cooling down, which can lead to a different nano-morphology as compared to annealing below the melting transition, where the changes in morphology are strongly based on the original film structure. This is also seen in the experimental results from a different PDPP4T batch (different molecular weight) as shown in Supporting Figure S11 (Supporting Information). However, despite these differences, also 300 °C -annealed films have increased crystalline regions and changed intermolecular distances with respect to non- and low-temperature-annealed films.

We also note a difference in ex situ and in situ GI-WAXS information. Specifically, in situ data had shown that below 150 °C, crystallite size is constant during cooling., while ex situ measurements show reduced FWHM. This could indicate that the observed changes in FWHM that are seen in ex situ GIWAXS data might be a result of
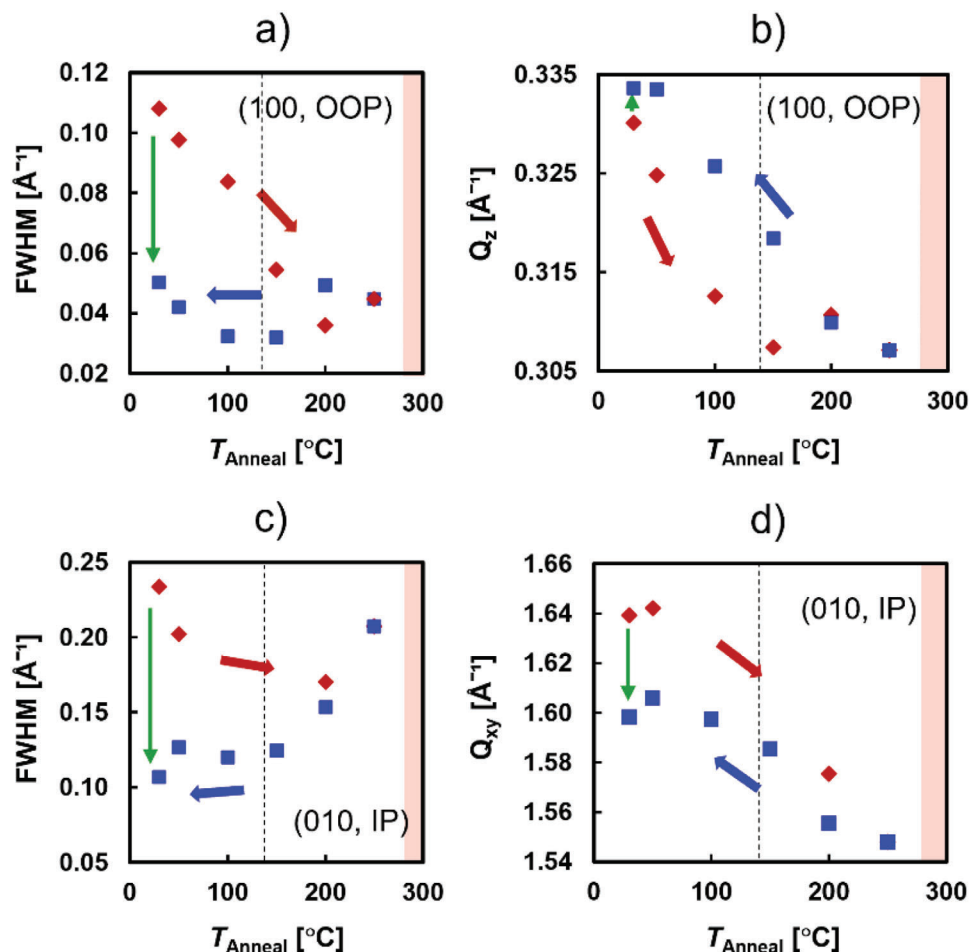
ADVANCED
SCIENCE NEWS

www.advancedsciencenews.com

ADVANCED
ELECTRONIC
MATERIALS
Open Access

www.advelectronicmat.de

Figure 3. In situ annealing (red symbols: heating, blue symbols: cooling) GIWAXS study of PDPP4T: FWHM and peak positions obtained from fitted 2D scattering images of PDPP4T films at different temperatures. The starting temperature for stability enhancement is marked by the dashed line. The red box indicates the region where the material starts to melt as determined from DSC. The green arrows highlight the change between the start and end of the heating & cooling cycle; a) FWHM of out-of-plane peak (100); b) peak position of out-of-plane peak (100); c) FWHM of in-plane peak (010); d) peak position of in-plane peak (010).

other effects, such as the release of contaminates or solvent residues.

We further studied the properties of high-temperature annealed films after spin-coating the original solvent chloroform. As can be seen in **Figure 4**, the crystallinity of films decreased after spin-coating chloroform. We further note that the solvent spin-coating process appears to cause a significant texture change with a larger fraction of face-on oriented polymer chains. When the solution stability test on the annealed films was immersion in the original solvent instead (see Figure S12, Supporting Information), the morphological changes were similar but even more pronounced. In order to see whether the morphological changes introduced by the solvent stability tests could be reversed, we re-annealed the films after exposure to their original solvent. From Figure 4, it can be seen that the texture of re-annealed PDPP4T films returned to the one of the films after the initial annealing, and that these films showed a further increased lamellar-stacking peak intensity compared to either, the 250°C annealed pristine and spin-coated film. This yet again

indicates that crystalline volume fraction in the sample increased by annealing.

2.2.2. AFM Study

AFM measurements were conducted to study the surface morphology of the polymer thin films. **Figure 5** shows AFM images of differently annealed PDPP4T thin films. We note that besides the slight increase in roughness (see Table S1, Supporting Information), it is difficult to note any major changes between non-annealed films and films annealed at temperatures up to 200 °C. In other words, the film changes that lead to the significant decrease in dissolubility of the films are not evident in the surface morphology of the films. However, films annealed at 250 and 300 °C exhibit a noticeably different morphology with a rather uniformly dimensioned grain-like structure with sizes in the tens of nanometer range. The almost spherical structures are slightly larger for the
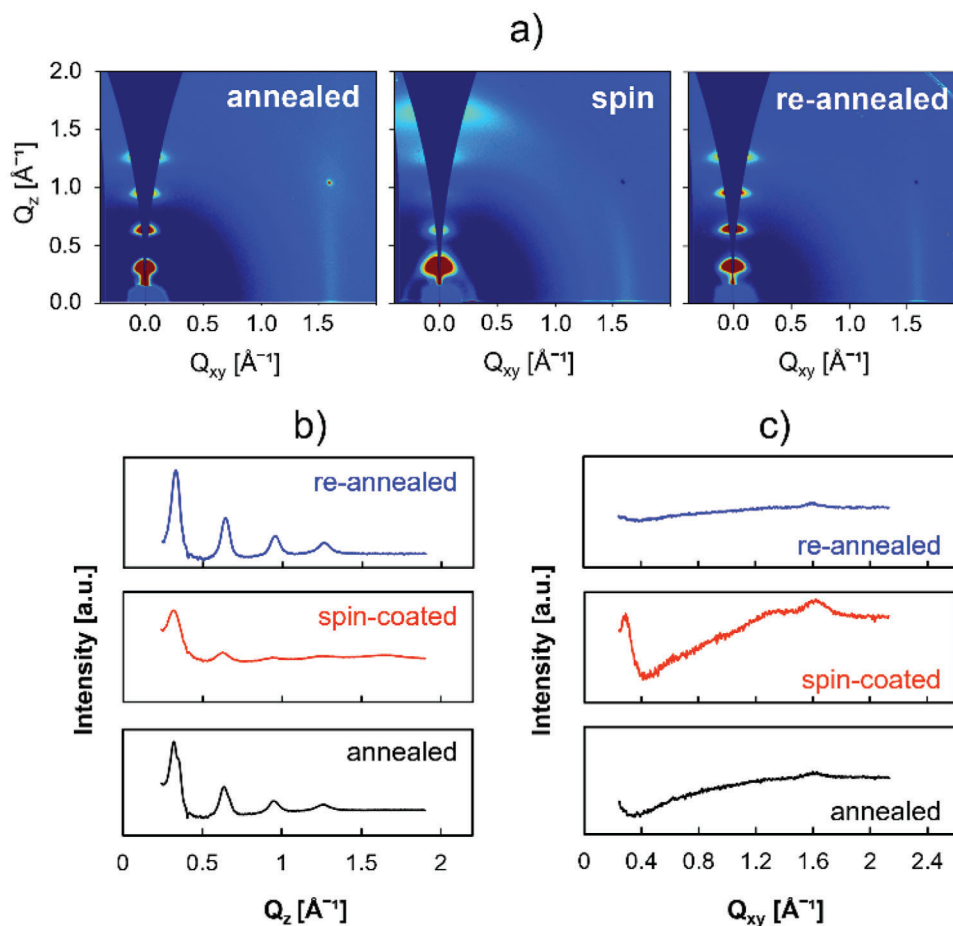
**ADVANCED
SCIENCE NEWS**

www.advancedsciencenews.com

**ADVANCED
ELECTRONIC
MATERIALS**

www.advelectronicmat.de

Figure 4. a) 2D scattering images of pristine 250°C annealed PDPP4T film (left), chloroform spin-coated film (middle), and 250°C-re-annealed film (right) obtained by GIWAXS measurement, b) out-of-plane line cuts, c) in-plane line cuts of the 2D scattering images in (a).

300 °C-annealed films and ≈30 to 40 nm in size. A similar observation has been made by Yang et al.[35] It is noticeable that this morphology forms relatively fast and can be observed after 1 min of annealing (Figure S13, Supporting Information). Moreover, it seems interesting to note that these are the films that showed very high resistance against the original solvent (regime III).

We also studied the film morphology after the retention test. After spin-coating the original solvent (Figure 5h,i), the surface morphology of high-temperature-annealed films again changed. While the film retains its initial thickness, the surface appears less rough with a fiber-like structure, as observed for low-temperature- and non-annealed films. In the case of 300°C-annealed films (Figure 5g,h), single grain-like structures are retained, but most of the films appear to be comprised of small fibers. As for the 250 °C-annealed film, the grain-like morphology completely disappeared after spin-coating and the film exhibits a morphology greatly resembling the one annealed at lower temperature, but with even lower roughness. Figure 5i–l further compares the high-temperature-annealed films after immersion and re-annealing. It is visible that films that were immersed in the original solvent appear almost featureless. After re-annealing, the granular morphology is recovered, but structure sizes are

overall smaller. We further note that immersion in the orthogonal solvent Propylene glycol monomethyl ether acetate (PGMEA) (Figure 5k) does not affect the surface morphology.

2.2.3. UV–Vis Absorption Spectroscopy

We further study our films via UV–vis absorption spectroscopy. The spectra of different temperature-annealed PDPP4T films are plotted in **Figure 6**. We observe a spectrum with an absorption band located at 790 nm (0-0 peak) and a vibronic shoulder at 720 nm (0-1 peak). The relative intensities of the 0-0 and 0–1 transitions being greater than unity suggest that all films are predominantly J-aggregated.[44] Upon the increase of annealing temperature above 50 °C, one can observe a minor but gradual red shift of the 0-0 absorption band. It is further noted that this red shift is accompanied by the narrowing of the 0-0 transition and the simultaneous emergence of the 0–1 transition from a rather faint into a pronounced shoulder as the temperature increases. This emergence of vibronic features is interpreted as enhanced aggregation[45] and is also observed in the AFM images. The small red shift of the 0-0 peak suggests a higher degree of molecular order[44] and it could be further
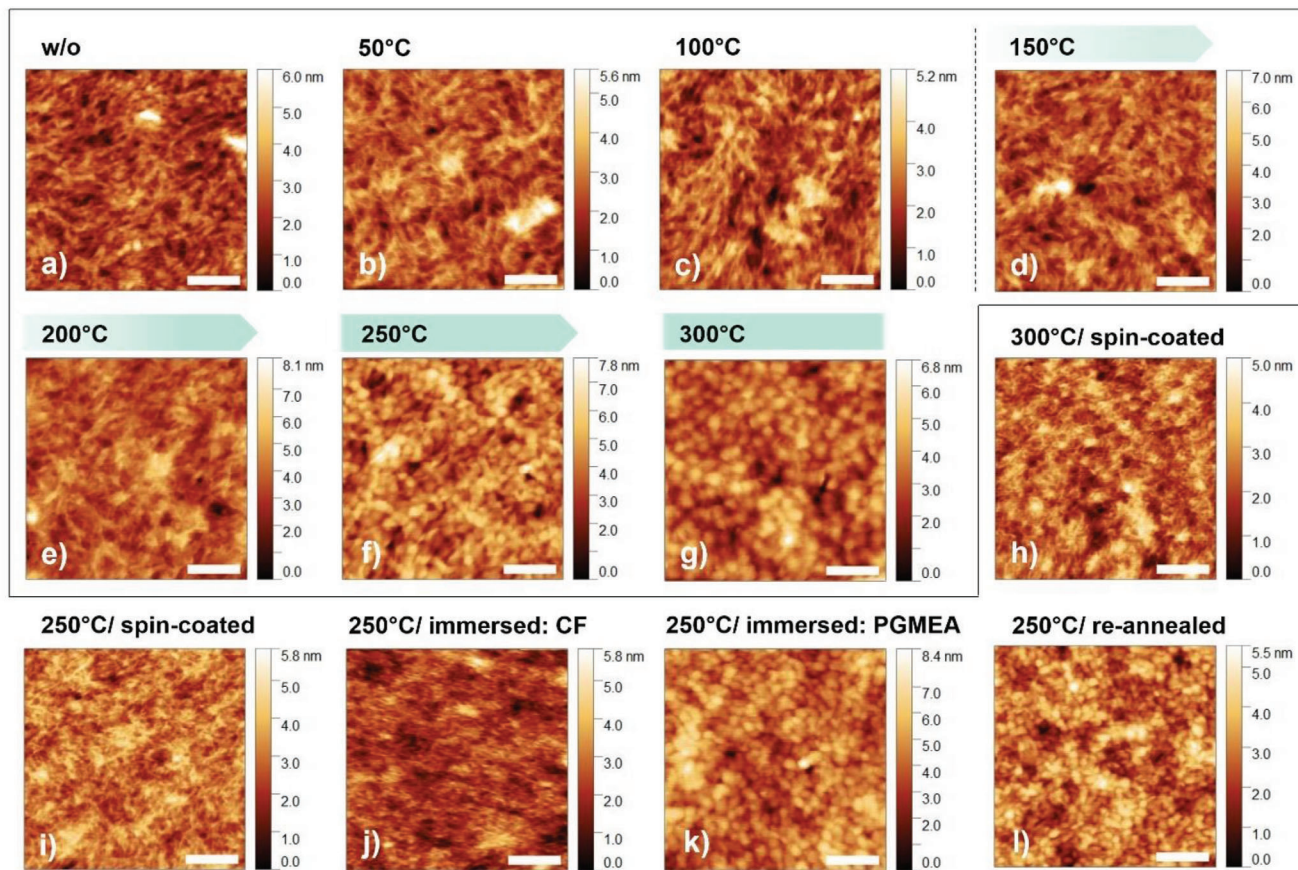
**ADVANCED
SCIENCE NEWS**

www.advancedsciencenews.com

**ADVANCED
ELECTRONIC
MATERIALS**

www.advelectronicmat.de

Figure 5. AFM images: non-annealed (original) PDPP4T film a) and films annealed at different temperatures b–g), high-temperature-annealed films after spin-coating the original solvent chloroform without re-annealing h,i) and comparison of 250 °C-annealed films after spin-coating i) and immersion j) in the original solvent chloroform, after immersion in the orthogonal solvent PGMEA k) and after re-annealing the original-solvent-immersed film l); all scale bars: 100 nm.

assumed that the polymer chains are less twisted, which increases the average effective conjugation length (increased intrachain order). Notably, at 300 °C the 0-0 peak shifts back, while the value is still above the one of non- and low-temperature-annealed films. At an annealing temperature of 300 °C, we further notice the sudden decrease of the 0-0 to 0–1 transition intensity ratio, which points to decreased intrachain coupling in these films,[44,46,47] and can further be interpreted as an increase in H-like aggregation.[48] This observation would be consistent with the possible onset of melting, which can give rise to more pronounced structural re-organization in those films.

We further study the films after spin-coating chloroform and after re-annealing for the same example as in the GI-WAXS comparison. Figure 6b compares the UV–vis-NIR data of high-temperature-annealed films to non-annealed films, the ones exposed to chloroform, and films that were subsequently re-annealed. It is observed that the peak at around ≈790 nm is blue-shifted after spin-coating chloroform and after re-annealing, the peak shows again a redshift. We further notice that the reannealed film has a decreased 0-0/0-1 intensity ratio, again pointing to the increase in H-like aggregation.[48]

2.3. Summary of Results and Interpretation

To summarize, several important observations were made for the temperature range that leads to increased solvent resistance (>140 °C) and that are common for all samples heated in this temperature range. First, the stability-improved films have overall larger grains, and second, their intermolecular distances are changed. Furthermore, a change in texture is observed.

The microstructural changes of the films during the annealing process are schematically summarized in **Figure 7a**. In general, all films are clearly textured and predominantly edge-on oriented. However, at low temperatures, when the samples were not heated or heated below the reported T_g (examples 30 °C and 50 °C), the predominantly edge-on stacked films, have a less pure texture with some signature of face-on orientation (phase I). Even when the films were heated below T_g, the decrease of the fitted FWHM is observed in the GIWAXS measurements, which might be attributed to the release of solvent residue or other impurities during low-temperature annealing. Especially given the fact that we used chloroform for thin film deposition, it is likely that 50 °C is enough to release its residues. As the samples are further heated beyond the reported T_g, chain segments in the amorphous phase gain mobility – with the portion and mobility
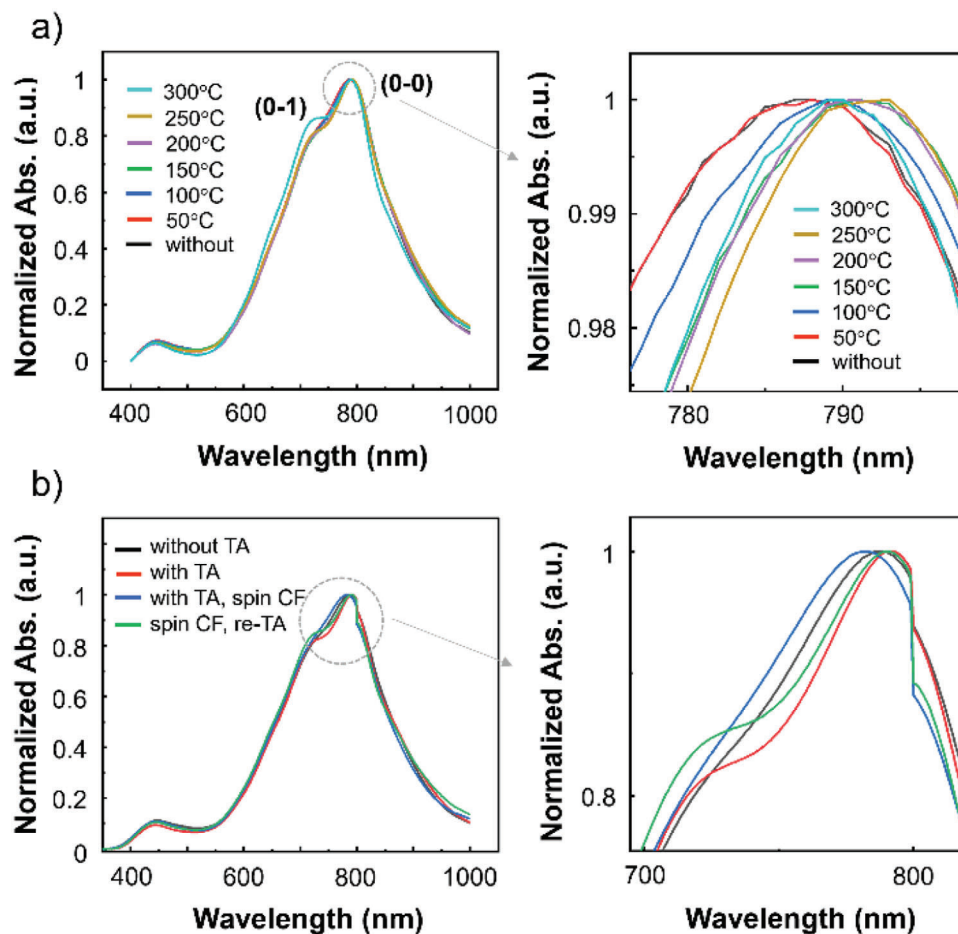
**ADVANCED
SCIENCE NEWS**

www.advancedsciencenews.com

**ADVANCED
ELECTRONIC
MATERIALS**

www.advelectronicmat.de

Figure 6. UV–vis–NIR absorption spectra of a) PDPP4T films after annealing at different temperatures. On the right, enlarged UV–vis absorption spectra, b) comparison of UV–vis absorption spectra of pristine (without TA) PDPP4T thin-film, 250 °C-annealed film (with TA), film after spin-coating chloroform (with TA, spin CF) and 250 °C re-annealed film (spin CF, re-TA), enlarged UV–vis absorption spectra are shown on the right.

increasing as the temperature is raised. It is observed that for samples that were heated just above the reported T_g value, grains that were oriented face-on re-arrange into an edge-on orientation and hence, more ordered lamellae are formed with the out-of-plane peak width accordingly reducing, which is seen during in situ heating too (phase II). We further observe the increase in both π–π and lamellar stacking distances. This thermal expansion is consistent with other studies[35,49] and reaches its maximum at the highest in situ heating temperature of 250 °C (phase III). As the film is cooled down (phase IV) and starts to contract, both, the π–π and lamellar packing distances reduce, and the reorganization of polymer chains results in a film with overall larger crystallites as compared to a non-annealed film, which is also supported by our UV–vis absorption spectroscopy results. Furthermore, the final lamellar distance is slightly reduced, while the π–π distance is increased (phase V). We suggest that these induced changes in morphology and crystallinity are at least partially the origin of the enhanced solvent resistance in a possible manner that is schematically depicted in Figure 7b.

Given the absence of proof for any chemical changes, we suggest that the slower solvent permeation of films that could result from the increase of crystalline regions could reduce the dis-

solution speed of these high-temperature-annealed films compared to non-annealed and low-temperature annealed films.[50] Furthermore, we hypothesize that as the crystallites grow in size, the chance of the amorphous phase getting confined at crystal interfaces might increase, which could mean that rigid amorphous phase might form or increase in fraction. Consequently, chain motion would be even more restricted (as compared to the situation where there is only mobile amorphous phase and crystallites), and dissolution might therefore proceed slower. This hypothesis somewhat aligns with the experimental observations and the general finding of the existence of rigid and mobile amorphous phases in similar Diketopyrrolopyrrole-based polymers,[36] as well as with the reports of several glass transition temperatures of this particular material.[30] However, in-depth studies of thermal behavior are needed to obtain direct proof for such mechanisms.

It was further noted that the lamellar ordering is enhanced. It might be speculated that the changed spatial distribution of very mobile side chains and rigid backbones affects the solvent permeation pathways. Furthermore, conformational changes and changes in the aggregated structure could very well slow down the dissolution process by introducing changes in the relative
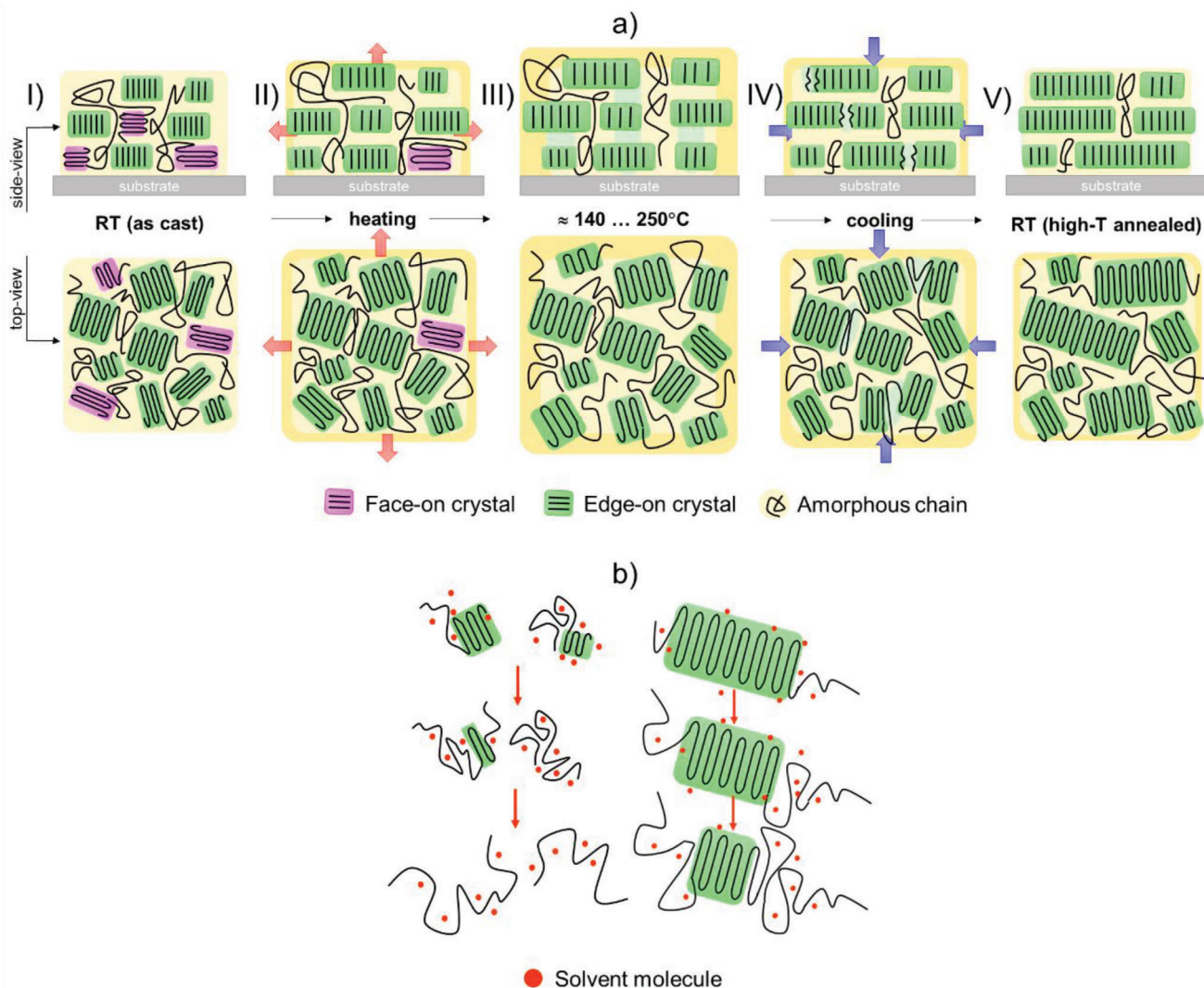
**ADVANCED
SCIENCE NEWS**

www.advancedsciencenews.com

**ADVANCED
ELECTRONIC
MATERIALS**

www.advelectronicmat.de

Figure 7. a) schematic drawing of the films´ evolution during high-temperature annealing: original film (I), re-orientation of grains (I → II), thermal expansion (I → III), enhanced lamellar order (II → III), contraction upon cooling (III → V), growth of crystallites (IV), high-T-annealed film with changed intermolecular spacings (V); b) schematic drawing of the suggested mechanisms responsible for changed dissolution behavior.

attractive forces between solvent and polymer.[51] Further investigations to shed light on the mechanism are currently on the way.

2.4. OFETs and Possible Impact on Polymer-Based Electronics

The possibility of changing the resistance of a material against its dissolution in a particular solvent can have a major impact on the ability to fabricate electronic devices that are based on functional polymers. Especially the simplicity of the presented approach makes it an attractive method for device fabrication where materials that have similar solubility need to be deposited sequentially on top of each other as is the case for various electronic devices such as memories, diodes, or specific transistor architectures. However, the strategies for increasing solvent resistance are only meaningful if the electronic properties are also preserved. To assess that and ob-

tain an understanding of the impact of high-temperature annealing on the electronic properties of films we BGTC OFETs.

The results are summarized in **Figure 8**. Figure 8a compares the transfer characteristics of devices with differently treated semiconducting films and calculated saturation mobilities are given in Figure 8b. The corresponding output characteristics are shown in Figure 8c. As can be seen, non-annealed and high-temperature annealed films show almost identical characteristics with the annealed films having slightly improved characteristics. After immersion of the annealed films in chloroform, the original solvent, a decrease in performance is observed. This change of characteristics upon immersion is easily explained by the change in nanomorphology that was observed above after films were exposed to their original solvent. However, if the films are re-annealed, the performance is not only recovered but distinctly improved even with respect to both the other films,
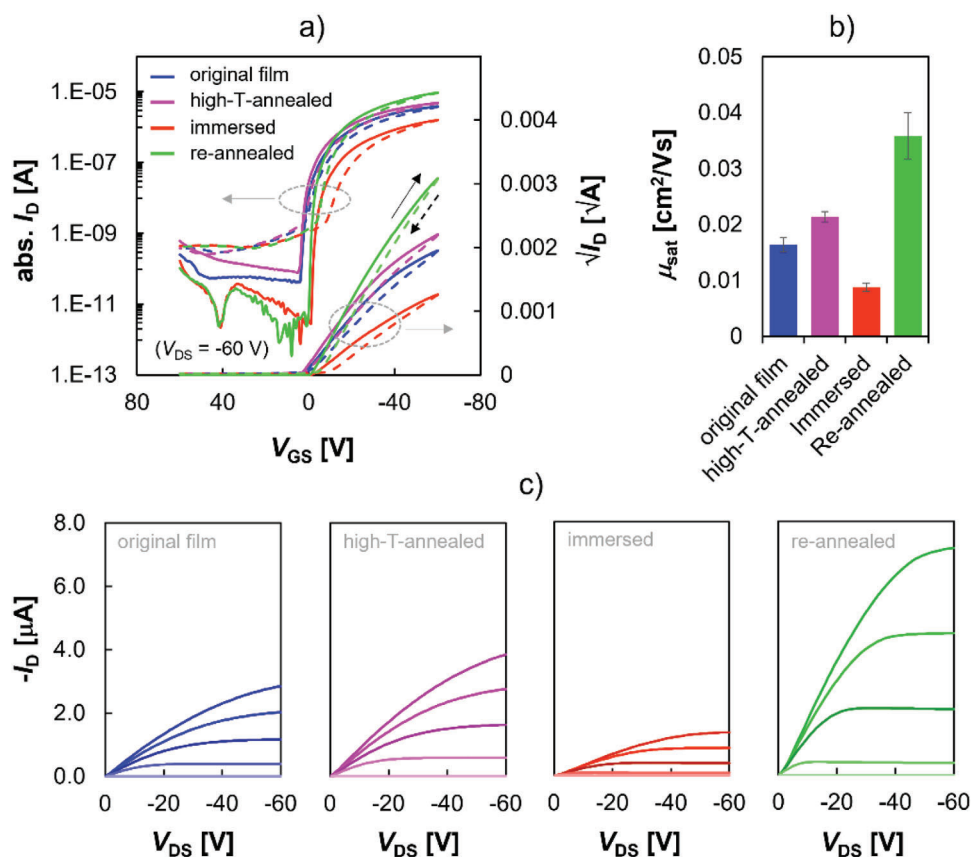
**ADVANCED
SCIENCE NEWS**

www.advancedsciencenews.com

**ADVANCED
ELECTRONIC
MATERIALS**

www.advelectronicmat.de

Figure 8. a) Transfer curves of PDPP4T devices based on original (= as shear-coated) films, high-temperature-annealed films (250 °C and 20 min), high-temperature-annealed films after immersion in original solvent (chloroform, 1 min) and same films after re-annealing (250 °C and 20 min). Solid and dashed lines correspond to transfer curves measured in forward (off to on) and reverse (on to off) direction, respectively. b) Extracted average saturation mobility values of BGTC OFETs with differently treated films, c) corresponding output characteristics.

i.e., non-annealed and high-temperature-annealed films. Despite these changes in mobility, we note that other device characteristics, such as the threshold voltage are almost unaffected, and even after immersion devices show overall decent FET characteristics.

Additional device data was obtained through similar tests but different annealing times (Figure S14, Supporting Information). It can be seen that even at short annealing times, devices perform similarly as for 20 min and that at high TA temperatures, the increase of annealing time does not appear to be beneficial in terms of changes produced by solvent immersion. Furthermore, we compared initial device characteristics to those with films immersed for 24 h in chloroform (Figure S15, Supporting Information). Impressively, reasonable device characteristics are obtained, which reflects on the outstanding stability that is introduced by this simple annealing procedure.

In addition, we studied whether the performance is also retained when the original device mobility is already higher. For this purpose, we fabricated devices on octadecyltrimethoxysilane (ODTMS)-modified substrates (see Figures S16, Supporting Information) and find that also on ODTMS, high-temperature-annealed films, which were immersed in chloroform and re-annealed, outperform the devices comprising the original films.

Moreover, following the careful evaluation of the device data in the presence of non-idealities,[52] the mobility values of "stabilized", high-temperature-annealed films compare reasonably well to the reported literature (see Table S2, Supporting Information). In addition, it is pointed out here that device testing was carried out for the most stable films that retain film thickness even after prolonged solvent exposure (TA = 250 °C), while the mobility is highest when the original film was annealed at 150 °C. In any case, the results show that high-temperature annealing cannot only enhance the resistance of the polymer semiconducting film against its original solvent but also preserves its performance.

To further corroborate the possible impact of thermal annealing for the fabrication of multi-layer devices, we also fabricated top-gate, bottom-contact (TGBC) OFETs where we deposit the dielectric from the same solvent that was used to prepare the polymer semiconductor layer. As can be seen in Figure S17 (Supporting Information), the devices perform well despite the use of the identical solvent for semiconductor and dielectric.

Therefore, we believe this simple method could be one step toward the realization of multi-layer polymer devices. Further investigations in this direction with first promising results are currently being carried out.
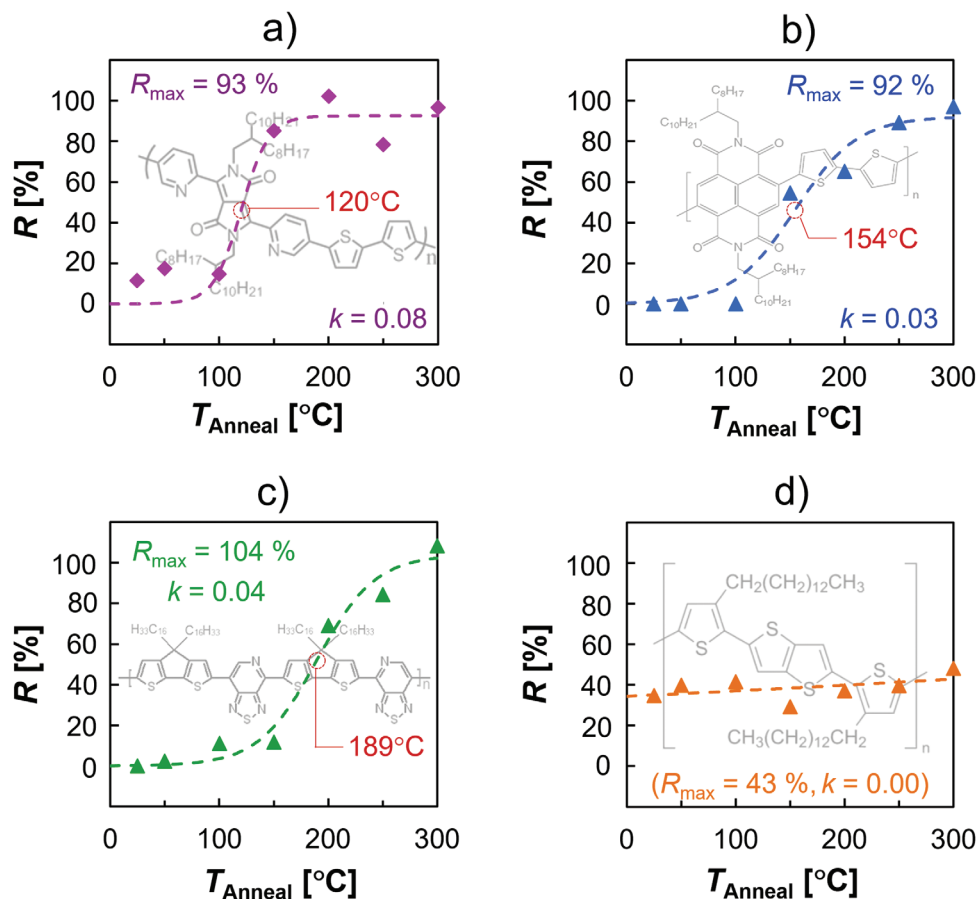
**ADVANCED
SCIENCE NEWS**

www.advancedsciencenews.com

**ADVANCED
ELECTRONIC
MATERIALS**

www.advelectronicmat.de

Figure 9. Thickness retention R (spin-coating test) dependent on annealing temperature for different polymer semiconductors: a) DPPDPyBT, b) N2200, c) PCDTPT and d) PBTTT, the insets show the chemical structures of the materials. The red circles mark the T_{50} temperature.

2.5. Extension to Other Polymers

Finally, we conducted initial experiments on the effect of thermal annealing on the solvent resistance of other commercially available polymer semiconductors. **Figure 9** shows the thickness retention over the annealing temperature for the polymers Poly(2,5-bis(2-octyldodecyl)−3,6-di(pyridin-2-yl)-pyrrolo[3,4-c]pyrrole-1,4(2H,5H)-dione-alt-2,2′-bithiophene) (DPPDPyBT), poly{[N,N′-bis(2-octyldodecyl)-naphthalene-1,4,5,8-bis(dicarboximide)−2,6-diyl]-alt-5,5′-(2,2′-bithiophene)} (N2200), poly[4-(4,4-dihexadecyl-4H-cyclopenta[1,2-b:5,4-b′]-dithiophen-2-yl)-alt-[1,2,5]thiadiazolo-[3,4-c]pyridine] (PCDTPT) and Poly[2,5-bis(3-tetradecylthiophen-2-yl)thieno[3,2-b]thiophene] (PBTTT).

Interestingly, we see that all the polymers except PBTTT undergo a change in the solvent resistance with the increase in annealing temperature leading to maximum fitted retention R_{max} greater than 90%. Furthermore, the T_{50} temperature of DP-PDPyBT is lower than the one observed for PDPP4T, while it is higher for N2200 and PCDTPT. Moreover, the change from no to maximum retention (as indicated by the growth rate k) appears to proceed over differently wide temperature ranges. It is also noted that PBTTT films do not completely dissolve even when not annealed. This behavior could relate to the overall poor solubility

at room temperature seen for this material or the interdigitation of side chains at room temperature.[53] Moreover, with PBTTT being the only material with linear side chains, a first and obvious assumption is that branched side chains are a prerequisite for the distinct change of dissolution behavior. However, other factors such as the thermal expansion coefficient, the characteristic initial morphology and distribution of crystalline and different amorphous phases, backbone rigidity, or the density of side chains could play an important role. Hence, we conclude that thermal physical cross-linking can be extended to other polymer semiconductors, but further studies are necessary to shed light on the required polymer characteristics that enable this simple thin film stabilization strategy.

3. Conclusion

In summary, we reported on the impact of thermal annealing on the resistance of the commercial semiconducting polymer PDPP4T against its original solvent. Based on a detailed study including AFM, GIWAXS, and UV–vis absorption spectroscopy, we proposed a mechanism to explain the reason behind the film's robustness change, which we believe is caused by the physical changes of the thin film. Finally, we studied this effect, which we termed "thermal physical cross-linking (TPC) effect",

**ADVANCED
SCIENCE NEWS**

www.advancedsciencenews.com

**ADVANCED
ELECTRONIC
MATERIALS**

www.advelectronicmat.de

regarding its impact on the electronic properties of the semiconducting thin films. For this purpose, we fabricated organic field-effect transistors and were able to show that TPC not only preserved the thin film when exposed to its original solvent but simultaneously retained the electronic properties. Initial studies on other semiconducting polymers further suggest that this method could be extended to other relevant materials. Hence, we believe that this simple and effective method could contribute to the development of polymer-based electronics.

4. Experimental Section

Chemicals: Poly{[N,N′-bis(2-octyldodecyl)-naphthalene-1,4,5,8-bis(dicarboximide)−2,6-diyl]-alt-5,5′-(2,2′-bithiophene)} (N2200) (molecular weight M_w = 132.27 Kg mol^{-1}), poly[2,5-bis(2-octyldodecyl)pyrrolo[3,4-c]pyrrole-1,4(2H,5H)-dione-3,6-diyl)-alt-(2,2′;5′,2′′;5′′,2′′′-quaterthiophen-5,5′′′-diyl)] (PDPP4T) (molecular weight M_w = 84.446 Kg mol^{-1} and M_w = 61.581 Kg mol^{-1}), and poly(2,5-bis(2-octyldodecyl)−3,6-di(pyridin-2-yl)-pyrrolo[3,4-c]pyrrole-1,4(2H,5H)-dione-alt-2,2′-bithiophene) (DPPDPyBT) (molecular weight M_w = 113.973 Kg mol^{-1}) were purchased from Ossila Ltd. Poly[4-(4,4-dihexadecyl-4H-cyclopenta[1,2-b:5,4-b′]-dithiophen-2-yl)-alt-[1,2,5]thiadiazolo-[3,4-c]pyridine] (PCDTPT) was purchased from 1-material. Poly[2,5-bis(3-tetradecylthiophen-2-yl)thieno[3,2-b]thiophene] (PBTTT-C14) (molecular weight M_w = 65 Kg mol^{-1}) was purchased from Sigma–Aldrich.

Thin Film Preparation: All films were deposited by shear coating using a custom-built laboratory setup. The semiconductors N2200, PCDTPT, DPPDPyBT, and PDPP4T were deposited from solutions in chloroform with the following concentrations: 8 mg mL^{-1} N2200, 8 mg mL^{-1} PCDTPT, 8 mg mL^{-1} DPPDPyBT, and 10 mg mL^{-1} or 12 mg mL^{-1} for the higher or lower molecular weight respectively. PBTTT was deposited from a 15 mg mL^{-1} solution in 1,2-di-chlorobenzene. The coating speeds were 2000, 1000, 1000, 2000, and 2000 um s^{-1} for N2200, PCDTPT, PBTTT, DPPDPyBT, and PDPP4T, respectively. The stage temperature was kept at 25 °C. A blade angle of 8° and a distance between the blade and substrate of 20 μm were kept throughout all coatings. All films were annealed in a glovebox in an N$_2$ atmosphere (<0.1 ppm O$_2$).

Thermal Properties: DSC was performed using a DSC2500 (by TA Instruments) with a heating/cooling rate of 10 K min^{-1} under nitrogen from −80 to 350 °C. TGA was conducted with a TGA Q5000 (by TA instruments) with a heating rate of 10 K min^{-1} from 25 to 800 °C under nitrogen.

Film Characterization: UV–vis–NIR absorption spectra were obtained by using a Cary 5000 (Agilent) spectrophotometer. The baseline-subtracted spectra were normalized by setting the maximum intensity to 1 and the lowest intensity to zero. Raman spectra were obtained using a confocal Raman microscope (Alpha300R, WITec) with an excitation laser wavelength of 532 nm at room temperature. The spectra were normalized to the substrate peak (SiO$_2$) located at 520 cm^{-1}. Optical microscopy pictures were captured with a Motic BA310Met optical microscope. Atomic force microscopy (AFM) images were obtained in tapping mode with Nanosurf FlexAFM and processed with Gwyddion 2.59 data visualization and analysis tool. Film thickness was measured with a profilometer (DektakXT, Bruker). Fourier transform infrared (FT-IR) spectroscopy was performed on the polymer thin films with a Spectrometer (Bruker optics, ALPHA-E) in 500–4000 cm^{-1} in ambient conditions. GIWAXS measurements were performed at the Sirius beamline at the SOLEIL synchrotron in Paris, France. The beam energy for the measurements was 10 keV. The sample–detector distance and the beam center were determined by using a lanthanum hexaboride reference. The measurements were performed in a helium atmosphere. The grazing incidence angle for all ex situ measurements was 0.14°. During in situ measurements, the angle was 0.1°. For all measurements, the samples were exposed to the beam for 5 × 30 s. GIWAXS data of solvent spin-coated, immersed and re-annealed samples were performed at the BL11 NCD-SWEET beamline at ALBA synchrotron in Barcelona, Spain. For the measurements in Figure 4, the distance between the sample and the detector (LX255-HS, Rayonix) was 17 cm, and the energy was 12.4 keV. For the measurements shown in Figure S10 (Supporting Information), the sample-detector distance was 20 cm. The grazing incidence angle of all measurements was 0.12°. The collected images were calibrated with a chromium oxide calibration standard. The 2D scattering data were analyzed with WxDiff software. For all GIWAXS measurements, the beam was in the direction parallel to the shear coating direction.

The robustness of the films against solvent exposure as would be needed for multi-layer deposition was tested with an emulated subsequent solution-deposition process. For the spin-coating test, the sample was covered with the respective solvent that was then spun off at 2000 rpm for 1 min. For the shear-coating test, the solvent was dropped onto the sample and "coated" with a speed of 2000 μm s^{-1}, which is in the typical range used for thin film deposition. For the soaking test (or dip-coating test), the sample was immersed in the original solvent for the duration of 1 min if not otherwise stated.

Device Fabrication: BGTC devices were fabricated on highly n-doped silicon wafers with a 300 nm SiO$_2$ layer in ambient conditions. After polymer thin film deposition, 50 nm thick Au source/drain electrodes were evaporated through a shadow mask. The channel length and width were nominally 100 and 1000 μm, respectively.

TGBC OFETs were prepared on cleaned glass substrates. Source and Drain electrodes (2.5 nm Cr/ 50 nm Au) were thermally evaporated. The channel length and width were 100 μm and 3000 μm, respectively. The polymethyl methacrylate (PMMA) dielectric layer was deposited from a 100 mg mL^{-1} solution in chloroform by shear-coating with a speed of 1000 μm s^{-1}. The PMMA films were annealed at 120 °C for 30 min. Finally, a PEDOT: PSS top-gate electrode was applied with a brush.

Electrical Characterization: The electrical characterization of fabricated OFETs was performed with a Keithley 4200A-SCS Parameter Analyzer in ambient conditions. Transfer characteristics were obtained by sweeping V_G between 60 and −60 V and reverse, and keeping V_D at −60 V. Average saturation mobility was calculated from the transfer characteristics with

$$\mu = 2L/WC_i(\partial\sqrt{|I_{DS}|}/\partial V_{GS})^2.$$

Supporting Information

Supporting Information is available from the Wiley Online Library or from the author.

Conflict of Interest

The authors declare no conflict of interest.

Data Availability Statement

The data that support the findings of this study are available from the corresponding author upon reasonable request.

[1] J. Song, H. Lee, E. G. Jeong, K. C. Choi, S. Yoo, *Adv. Mater.* **2020**, *32*, 1907539.

[2] C. Keum, C. Murawski, E. Archer, S. Kwon, A. Mischok, M. C. Gather, *Nat. Commun.* **2020**, *11*, 6250.

[3] Y. Lin, M. I. Nugraha, Y. Firdaus, A. D. Scaccabarozzi, F. Aniés, A. H. Emwas, E. Yengel, X. Zheng, J. Liu, W. Wahyudi, E. Yarali, H. Faber, O. M. Bakr, L. Tsetseris, M. Heeney, T. D. Anthopoulos, *ACS Energy Lett.* **2020**, *5*, 3663.

[4] W. Li, Y. Xu, X. Meng, Z. Xiao, R. Li, L. Jiang, L. Cui, M. Zheng, C. Liu, L. Ding, Q. Lin, *Adv. Funct. Mater.* **2019**, *29*, 1808948.

[5] A. Wadsworth, Z. Hamid, J. Kosco, N. Gasparini, I. McCulloch, *Adv. Mater.* **2020**, *32*, 2001763.

[6] W. Li, F. Guo, H. Ling, P. Zhang, M. Yi, L. Wang, D. Wu, L. Xie, W. Huang, *Adv. Sci.* **2017**, *4*, 1700007.

[7] H. W. Park, K. Y. Choi, J. Shin, B. Kang, H. Hwang, S. Choi, A. Song, J. Kim, H. Kweon, S. Kim, K. B. Chung, B. S. Kim, K. Cho, S. K. Kwon, Y. H. Kim, M. S. Kang, H. Lee, D. H. Kim, *Adv. Mater.* **2019**, *31*, 1901400.

[8] C. Zhang, S. Holdcroft, *J. Mater. Res.* **2018**, *33*, 1879.

[9] C. Y. Nam, Y. Qin, Y. S. Park, H. Hlaing, X. Lu, B. M. Ocko, C. T. Black, R. B. Grubbs, *Macromolecules* **2012**, *45*, 2338.

[10] S. Sax, N. Rugen-Penkalla, A. Neuhold, S. Schuh, E. Zojer, E. J. W. List, K. Müllen, *Adv. Mater.* **2010**, *22*, 2087.

[11] A. M. Gaikwad, Y. Khan, A. E. Ostfeld, S. Pandya, S. Abraham, A. C. Arias, *Org. Electron.* **2016**, *30*, 18.

[12] A. Nyayachavadi, A. Langlois, M. N. Tahir, B. Billet, S. Rondeau-Gagné, *ACS Appl. Polym. Mater.* **2019**, *1*, 1918.

[13] M. H. Petersen, S. A. Gevorgyan, F. C. Krebs, *Macromolecules* **2008**, *41*, 8986.

[14] P. J. Leenaers, M. M. Wienk, R. A. J. Janssen, *Org. Electron.* **2020**, *86*, 105914.

[15] P. Panayotatos, D. Parikh, R. Sauers, G. Bird, A. Piechowski, S. Husain, *Sol. Cells* **1986**, *18*, 71.

[16] A. Tamayo, T. Kent, M. Tantitiwat, M. A. Dante, J. Rogers, T. Q. Nguyen, *Energy Environ. Sci.* **2009**, *2*, 1180.

[17] K. Gu, Y. Wang, R. Li, E. Tsai, J. W. Onorato, C. K. Luscombe, R. D. Priestley, Y. L. Loo, *ACS Appl. Mater. Interfaces* **2021**, *13*, 999.

[18] N. H. Yusof, N. I. A. Azes, S. Buniran, *Adv. Mater. Res.* **2014**, *879*, 144.

[19] M. Li, A. H. Balawi, P. J. Leenaers, L. Ning, G. H. L. Heintges, T. Marszalek, W. Pisula, M. M. Wienk, S. C. J. Meskers, Y. Yi, F. Laquai, R. A. J. Janssen, *Nat. Commun.* **2019**, *10*, 2867.

[20] V. A. Pozdin, D. M. Smilgies, H. H. Fong, M. Sorensen, M. He, *J. Mater. Chem. C* **2016**, *4*, 5255.

[21] F. Talnack, S. Hutsch, M. Bretschneider, Y. Krupskaya, B. Büchner, M. Malfois, M. Hambsch, F. Ortmann, S. C. B. Mannsfeld, *Mol. Syst. Des. Eng.* **2022**, *7*, 507.

[22] A. Luzio, J. Martin, C. H. Cheng, N. Stingelin, M. F. Toney, A. Salleo, M. Caironi, *J. Mater. Chem. C* **2021**, *9*, 15848.

[23] T. T. Ngo, D. N. Nguyen, V. T. Nguyen, *Adv. Nat. Sci. Nanosci. Nanotechnol.* **2012**, *3*, 045001.

[24] J. Liu, T. F. Guo, Y. Yang, *J. Appl. Phys.* **2002**, *91*, 1595.

[25] H. Cha, J. Li, Y. Li, S.-O. Kim, Y.-H. Kim, S.-K. Kwon, *Macromol. Res.* **2020**, *28*, 820.

[26] G. Li, V. Shrotriya, Y. Yao, Y. Yang, *J. Appl. Phys.* **2005**, *98*, 043704.

[27] Y. Li, P. Sonar, S. P. Singh, M. S. Soh, M. van Meurs, J. Tan, *J. Am. Chem. Soc.* **2011**, *133*, 2198.

[28] K. Y. Ryu, J. Lee, T. Jun, D. Lee, B. Kim, D. Y. Ryu, K. Kim, *ACS Appl. Mater. Interfaces* **2022**, *14*, 23474.

[29] B. Liu, R.-Q. Png, L.-H. Zhao, L.-L. Chua, R. H. Friend, P. K. H. Ho, *Nat. Commun.* **2012**, *3*, 1321.

[30] P. Jarka, B. Hajduk, T. Tański, H. Bednarski, H. Janeczek, P. Gnida, M. Fijalkowski, *SSRN Electron. J.* **2022**, *15*, 8392.

[31] Y. Furushima, M. Nakada, K. Ishikiriyama, A. Toda, R. Androsch, E. Zhuravlev, C. Schick, *J. Polym. Sci. Part B Polym. Phys.* **2016**, *54*, 2126.

[32] Y. Furushima, C. Schick, A. Toda, *Polym. Cryst.* **2018**, *1*, 10005.

[33] C. Schick, *Anal. Bioanal. Chem.* **2009**, *395*, 1589.

[34] Z. Qian, L. Galuska, W. W. McNutt, M. U. Ocheje, Y. He, Z. Cao, S. Zhang, J. Xu, K. Hong, R. B. Goodman, S. Rondeau-Gagné, J. Mei, X. Gu, *J. Polym. Sci. Part B Polym. Phys.* **2019**, *57*, 1635.

[35] L. Yang, Y. Wu, Y. Yan, Z. Wang, Y. Qiao, D. Chang, C. Zhang, Y. Wang, X. Lu, Y. Liu, Y. Zhao, *Adv. Funct. Mater.* **2022**, *32*, 2202456.

[36] S. Luo, T. Wang, M. U. Ocheje, S. Zhang, J. Xu, Z. Qian, X. Gu, G. Xue, S. Rondeau-Gagné, J. Jiang, W. Hu, E. Zhuravlev, D. Zhou, *Macromolecules* **2020**, *53*, 4480.

[37] J. Martín, N. Stingelin, D. Cangialosi, *J. Phys. Chem. Lett.* **2018**, *9*, 990.

[38] S. Zhang, A. Alesadi, M. Selivanova, Z. Cao, Z. Qian, S. Luo, L. Galuska, C. Teh, M. U. Ocheje, G. T. Mason, P. B. J. St. Onge, D. Zhou, S. Rondeau-Gagné, W. Xia, X. Gu, *Adv. Funct. Mater.* **2020**, *30*, 2002221.

[39] S. E. Root, M. A. Alkhadra, D. Rodriquez, A. D. Printz, D. J. Lipomi, *Chem. Mater.* **2017**, *29*, 2646.

[40] R. Xie, Y. Lee, M. P. Aplan, N. J. Caggiano, C. Müller, R. H. Colby, E. D. Gomez, *Macromolecules* **2017**, *50*, 5146.

[41] V. Savikhin, L. K. Jagadamma, L. J. Purvis, I. Robertson, S. D. Oosterhout, C. J. Douglas, I. D. W. Samuel, M. F. Toney, *iScience* **2018**, *2*, 182.

[42] S. Krimm, C. Y. Liang, G. B. B. M. Sutherland, *J. Chem. Phys.* **1956**, *25*, 549.

[43] J. Rivnay, R. Steyrleuthner, L. H. Jimison, A. Casadei, Z. Chen, M. F. Toney, A. Facchetti, D. Neher, A. Salleo, *Macromolecules* **2011**, *44*, 5246.

[44] M. Más-Montoya, R. A. J. Janssen, *Adv. Funct. Mater.* **2017**, *27*, 1605779.

[45] R. Heuvel, F. J. M. Colberts, J. Li, M. M. Wienk, R. A. J. Janssen, *J. Mater. Chem. A* **2018**, *6*, 20904.

[46] F. C. Spano, C. Silva, *Annu. Rev. Phys. Chem.* **2014**, *65*, 477.

[47] C. Hellmann, F. Paquin, N. D. Treat, A. Bruno, L. X. Reynolds, S. A. Haque, P. N. Stavrinou, C. Silva, N. Stingelin, *Adv. Mater.* **2013**, *25*, 4906.

[48] T. Sarkar, S. A. Schneider, G. Ankonina, A. D. Hendsbee, Y. Li, M. F. Toney, G. L. Frey, *Chem. Mater.* **2020**, *32*, 7338.

[49] J. Kuebler, T. Loosbrock, J. Strzalka, L. Fernandez-Ballester, *Macromolecules* **2023**, *56*, 3083.

[50] L. Rebenfeld, P. J. Makarewicz, H.-D. Weigmann, G. L. Wilkes, *J. Macromol. Sci. Part C* **1976**, *15*, 279.

[51] M. Gilbert, in *Brydson's Plastics Materials*, Elsevier, Amsterdam, Netherlands **2017**, pp. 75-102.

[52] H. H. Choi, K. Cho, C. D. Frisbie, H. Sirringhaus, V. Podzorov, *Nat. Mater.* **2018**, *17*, 2.

[53] D. M. DeLongchamp, R. J. Kline, Y. Jung, D. S. Germack, E. K. Lin, A. J. Moad, L. J. Richter, M. F. Toney, M. Heeney, I. McCulloch, *ACS Nano* **2009**, *3*, 780.